Measuring Size and Shape Heterogeneity in AAVs with Ion Mobility Mass Spectrometry

Ellen Liggett[1], Keith Richardson[2], David Langridge[2], Kevin Giles[2], Ian Anderson[3], Kamila Pacholarz[4], Paul Getty[4], Michael Walker[4], Jakub Ujma*[2], Perdita Barran*[1]

1. Michael Barber Centre for Collaborative Mass Spectrometry, Manchester Institute of Biotechnology, University of Manchester, UK
2. Waters Corporation, Wilmslow, UK
3. Lonza, Slough, UK
4. Pharmaron Biologics, Liverpool, UK

*Corresponding authors

Keywords: Ion Mobility, Mass Spectrometry, Travelling Wave, Drift Tube, Adeno-Associated Viruses, Gene Therapy

Abstract

Adeno-associated viruses (AAVs) are at the forefront of biopharmaceutical development as gene therapy vectors. The successful approval of these medicines requires robust characterization including an assessment of therapeutic gene content. Using ion mobility–mass spectrometry (IM-MS) techniques, we determine empty:full capsid ratios and explore structural differences in AAV particles relevant to payload. With drift tube IM-MS, we demonstrate that empty capsids, while slightly smaller, present more conformational variability than full capsids. This method also resolves two partially filled capsid species with intermediate masses, between that of empty and full capsids wherein the lower mass feature is conformationally more like empty and the higher mass feature appears highly similar to the full capsid. We present data using travelling wave ion mobility (TWIM) operated under conditions that limit or favour the mass-to-charge ratio (*m/z*) dependence on ion transit time through the drift cell *via* the velocity relaxation effect. This permits separation of empty and full capsids in the absence of mass spectrometry information, providing a new approach to study conformational and mass differences in super massive particles.

Graphical Abstract

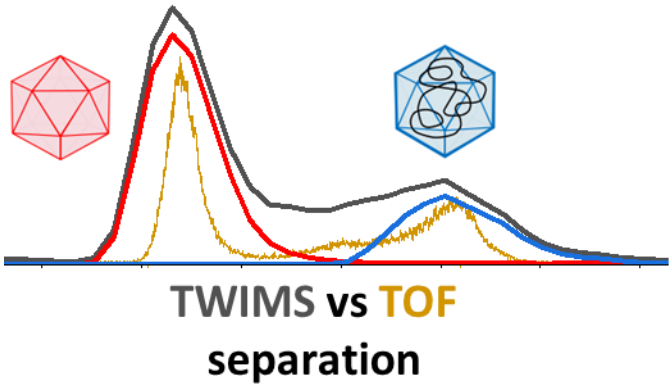

Introduction

Adeno-associated viruses (AAVs) are attractive targets as vectors for gene therapy; they have low immunogenicity and low pathogenicity as, to date, no isolated AAV serotype has caused infection to a human host.[1–3] The AAV capsid has a symmetrical T=1 icosahedral geometry and is composed of 60 subunits of three viral protein (VP) constructs: VP1, VP2 and VP3. The VPs are formed from the same mRNA transcript with alternative splice patterns, thus having

the same base sequence (VP3), with two additional N-terminal protein lengths derived from earlier open reading frame expression start points (VP2 and VP1).[4,5] The commonly reported average capsid VP ratio of 1:1:10 reflects relative concentrations of VP capsids in solution and corresponds to a mass of ~3.7 MDa.[6] Many human and primate AAV capsid serotypes have been identified that have different tissue tropisms due to diverse interactions with host cell receptors, which makes them increasingly attractive for more targeted gene therapy approaches.[7–9] AAVs cannot replicate without co-infection with other viruses and as such, recombinant AAV (rAAV) capsids are replication incompetent, with viral DNA removed.[3] For biopharmaceutical companies producing recombinant AAV (rAAV) gene therapies, development of robust characterisation methods that quantify the therapeutic gene content of the capsids is necessary to obtain approval from medicine agencies.[10,11] Processed samples are a heterogeneous mixture of viral capsids containing: an intact genome (full); capsids with no genome (empty); and capsids with a partial genome construct or hcDNA (partial). Additionally, we can observe overpackaged capsids where the contained genome is larger than the intended gene of interest (GOI). This could be multiple copies of a small GOI which does not reach the packaging capacity of the AAV capsid, thus more copies are inserted.[12,13] In addition, varying stoichiometries of the VP subunits in the assembled capsids provides more sample complexity.[14] Analytical ultra centrifugation (AUC), cryo-electron microscopy (EM), mass photometry and size exclusion chromatography with multi-angle light scattering (SEC-MALS) are all currently used for AAV sample characterisation.[15–17] These techniques can distinguish the ratios of the major capsid species but have limitations, such as requiring large sample volumes, cost of use, long measurement time scales or inability to distinguish partially-filled capsids.[18,19]

Mass spectrometry (MS) is a widely used analytical technique that requires low sample consumption, with the capability to examine intact, non-covalently bound species and provide useful structural information. As such it has increased applicability for the study of different classes of megadalton (MDa) sized biological complexes including intact viruses. Electrospray ionisation (ESI) permits gentle transfer of large biomolecules into the gas phase, maintaining non-covalent interactions such that these intermediate and native complexes can be studied.[20,21] Pioneering work over the past 20 years by Ashcroft, Heck, Jarrold, Robinson and Uetrecht, amongst others, has furthered the use of mass spectrometry to examine intact

viruses.[22–26] Much of this has focussed on development of methods and instrumentation to study assembly and report on intact stoichiometries including the bacteriophage MS2 capsid (2.5 MDa)[27], and the Prohead-1 capsid head from the HK97 bacteriophage (18 MDa).[28]

Hyphenated MS methods have also been employed including hydrogen deuterium exchange (HDX)-MS, which has been applied to study *in vitro* binding of monoclonal antibodies to hepatitis B virus (HBV) capsids.[29] Coupling to liquid chromatography (LC) prior to MS analysis can provide structural information on the primary sequence of viral capsid subunits, and such approaches are used to routinely characterise gene therapy products. An example of this is the use of hydrophilic interaction chromatography (HILIC) to identify VP variants from AAV serotypes as well as those that differ due to post-translational modifications (PTMs).[30]

The analytical challenges posed by large heterogenic assemblies, as well as the importance of such measurements have catalysed developments in charge detection (CD)-MS, in both purpose built and modified instruments.[31–33] Different pathways in the assembly of MDa HBV capsids were revealed by directly measuring the charge of the subunits and assembled intact species to then determine the mass-to-charge ratio (*m/z*).[24] For rAAVs, the VP assembly into the native capsid has recently been examined with CDMS using an Orbitrap and described as stochastic, resulting in capsids with a high degree of heterogeneity in VP ratio, where the most abundant capsids represents less than 2.5% of the total population.[34,35] Using an ion mobility enabled Q-ToF instrument fitted with an electron capture dissociation (ECD) device, individual reduced charge states of AAV5 have been resolved by employing electron-capture charge reduction, resulting in mass distributions.[36] A similar method was later employed on Orbitrap instrumentation to resolve individual charge states of AAV8.[37] Stability and dissociation of AAV capsids has been studied with a variable temperature (VT)-CDMS instrument, revealing that at high temperature full AAVs eject their genetic cargo first, forming empty capsids before final capsid dissociation into component VPs.[38] Additional CDMS work has explored possible truncations of the therapeutic gene content of rAAVs, significant in the characterisation of these gene therapy vectors.[39] Such complexities in the product pose a challenge for quality control and drug efficacy.

Large particles in IMS devices

In this report we focus on ion mobility spectrometry (IMS) technologies for analysis of AAV capsids. IMS measures the movement of ions through an inert buffer gas induced by the electric field. Two commonly used implementations of IMS are drift tube IMS (DTIMS) and travelling wave IMS (TWIMS). Both technologies are often coupled with MS detection (e.g. DTIM-MS and TWIM-MS) and have been reviewed extensively.[40,41] In DTIMS, a linear electric field (E) is applied across a drift tube of a given length. The mobility of ions (K) can be found by measuring their transit time through the tube. Under a so called 'low field limit',[42] the ions drift at their terminal velocities (v_D) and K is the proportionality constant between v_D and E:

$$v_D = KE \tag{1}$$

K depends on ions charge (q), buffer gas number density (N), temperature (T), reduced mass of ion and gas molecules (μ), as well as their collision cross section (CCS). The latter parameter informs on the conformational preferences of an ion. When used in conjunction with a mass spectrometer as a detector, the hybrid technique of DTIM-MS provides *m/z* as well as measurement of K, from which it is possible to estimate the CCS of the ion.[43]

$$CCS = \frac{3q}{16N}\sqrt{\frac{2\pi}{\mu k_B T}}\frac{1}{K} \tag{2}$$

Commonly, the mobility of an ion, and therefore it's CCS, is determined by taking a series of measurements at different field strengths, discussed elsewhere.[44,45] In recent decades, there have been significant developments in the application of DTIM-MS to increasingly larger molecules.[46]

The introduction of radio frequency (RF)-confinement[47] facilitated the efficient transmission of high-mass ions.[48,49] An RF-confining DTIMS cell was used to measure CCS values of a range of protein complexes, including the large ~801 kDa GroEL complex.[50] A similar device was used to study biopharmaceutical antibody collisional cross section distributions (CCSDs) to probe conformational spread.[51] A variable temperature (VT) DTIM-MS instrument utilising a modular linear drift cell surrounded by a cooling copper coil and a metal encapsulated resistive heater coil[52] explored the structural changes experienced by monomeric proteins at freezing temperatures in the gas phase[53] and was employed to study the conformational changes upon thermally activated dissociation of large protein complexes including serum

amyloid P component (SAP).[54] Despite these developments, there are no reports of the use of DTIM-MS to study native virus assemblies due to the difficulties in transmitting MDa species through such instruments.

TWIMS has a similar configuration to DTIMS, where ions drift in a cell in the presence of a gas under the influence of electric fields. However, TW-induced ion transport involves a perpetual cycle of acceleration and deceleration, where ions are pushed and overtaken by sequential waves.[55,56] During each cycle, ions will approach (but not reach) the terminal drift velocity dictated by their K. This 'velocity relaxation' effect has been encountered in the past, notably in the 'field reversing' experiments of Johnsen and Biondi, who correlated the relaxation time to the product of an ions' *m/z* and K.[57] Akin to this, the weak *m/z* dependence of TWIMS separation has been noted.[58] Consequently, calibration of standards with absolute mobilities previously determined *via* DTIMS is necessary to ascertain CCS values for analyte ions in a TWIMS cell, which can then be compared between different instruments and laboratories.[59]

TWIM-MS was commercialised almost 2 decades ago[61,62] and used extensively since to study high mass molecules. Devine *et al.* have reported that non-globular proteins may be less conformationally robust and hence be subject to gas-phase compaction within the TWIMS cell, leading to underestimation of the size and shape of the molecule compared to its native structure, similar effects have been noted for monoclonal antibodies and many other proteins and protein complexes.[63,64] The advantages of TWIM-MS to study viruses were apparent over ten years ago when it was used to monitor MS2 capsid assembly, whereby homo-dimer coat proteins form hexamer or decamer intermediates on the pathway to forming the full T=3 180 copy number capsid.[23] TWIM-MS was also applied to study the assembly of HBV and Norovirus capsids where molecular modelling software MOBCAL was used to validate experimental values.[65]

We have recently reviewed the use of IM-MS techniques in structural biology, emphasizing the significant increase in understanding of complex biomolecular structures and dynamics that these tools can provide.[40] With such heterogeneous analytes such as AAV capsids, the two-dimensional IM-MS analysis can aid in the discrimination between capsid species and provide additional attributes to support quality assurance of these gene therapy formulations. In this study we show the first analysis of AAVs with DTIMS, providing CCS

values for this serotype of capsid. Additionally, we utilise the velocity relaxation effect in TWIMS to explore TW-based K- versus *m/z*-dominated separations of empty and full AAVs.

Experimental Details

Sample preparation

AAV samples were provided by Pharmaron Ltd and produced *via* triple transient transfection of vector genome, AAV helper and Adenovirus helper plasmids into a suspension cell culture of HEK293 cells. The additional two samples containing different mixtures of full and empty AAV8 were obtained from UNC Vector Core and Lake Pharma. For IM-MS experiments, AAV samples were buffer exchanged into ammonium acetate (150 mM, pH 6.8-7.0) using Bio-Spin P-6 Gel Columns (Bio-Rad Laboratories, Hercules, CA, USA) according to the manufacturer's protocol. The final sample concentration was approximately $1e^{13}$ viral particles/mL as confirmed by dynamic light scattering (data not shown). All samples contained both empty and full capsids as is common following manufacture. 10 µL was loaded into either coated glass capillaries (PicoTip, NewObjective, USA) with 1P-4P coating and a tip size of 4 µm, or borosilicate glass capillaries pulled in-house with a platinum wire inserted into the sample to confer capillary voltage.

Ion Mobility Mass Spectrometry

IM-MS experiments were performed on a Synapt XS fitted with a nESI source (Waters, UK) with either a TWIMS or DTIMS cell installed. Source conditions were the same for both experiments and were as follows: capillary voltage was 1.2 kV, sampling cone was 50 V with a source offset of 2 V. Source temperature was 100°C with a desolvation temperature of 250°C. Drift gas pressure was measured at 2.2 mbar with the capacitance manometer (CDG025D, Inficon). For DTIMS, the arrival time distributions (ATDs) were recorded at five electric field strengths. The mobility was then extracted from the slope of linear relationship between the arrival time and electric field. Using the expected masses of full and empty AAV, we estimated the average charge of AAV ions from the mean *m/z* value of the charge state envelope. The expected mass, inferred charge and measured mobility were then used to calculate CCS values, using Mason Schamp equation.[43]

For TW-based separations, we used two sets of operating parameters resulting in low velocity relaxation ('K-dominated') and high velocity relaxation ('*m/z*-dominated'). K-dominated experiments used a TW velocity of 100 m/s and a TW height of 14 V. For *m/z*-dominated separations TW velocity was increased to 320 m/s and TW velocity set to 40 V.

A SELECT SERIES™ Cyclic IMS™ instrument was used for higher resolution TW separations. The source conditions were as above. Cyclic IMS cell (cIM) was operated with TW velocity of 375 m/s and TW height of 30 V, nitrogen pressure was measured at 1.8 mbar.

Data was analysed on MassLynx V4.2, Driftscope V2.9 and Origin 2021b. MassLynx was used to visualise the IM-MS data which was imported into Driftscope to produce the 2D IM-MS heatmaps. Extracted ATDs were taken for the different capsid species in the *m/z* ranges as follows: empty capsid 20,000-24,000 *m/z*; first partially filled capsid 24,000-26,500 *m/z*; second partially filled capsid 26,500-28,000 *m/z*; full capsid 28,500-32,000 *m/z*. Full width at half maximum (FWHM) values were calculated and plotted using Origin.

Simulations

SIMION (IMI Adaptas, US) was used to evaluate how ions, resembling AAVs, transmit through the Cyclic IM device, at a range of TW conditions and their *m/z* values. We simulated a range of hypothetical, spherical capsids of varying density (assuming the same average charge of 175 and radius of 125 Å). The Statistical Diffusion Simulation (SDS) model was used to approximate collisions of ions with the background gas (1.8 mbar N_2).[66]

Results and Discussion

DTIMS Analysis of AAV Capsids

Data from the DTIMS experiments are shown in Figure 1. In the *m/z* domain, two main peaks are observed at *m/z* ~22,000 and ~30,000. These are in agreement with the prior CDMS results[67] and assigned as charge state envelopes of full and empty capsids respectively. The individual charge state peaks cannot be discerned in the *m/z* domain due to the high average charge and mass heterogeneity of the capsid species as previously reported.[34] There are two minor peaks observed at *m/z* ~25,000 and ~27,000 and we have assigned these as 'partial 1' and 'partial 2', respectively. We assume that these are AAV capsids which did not incorporate the full-length transgene, or have incorrectly packaged hcDNA) when they were produced

and so are heterogeneous mixture containing incomplete AAV genomes, plasmid fragments or residual host cell DNA.[15] The region of low intensity ions below *m/z* 10,000 is possibly unresolved capsid proteins, for example the most abundant VP3.

The benefit of performing both IM and MS means it is possible to extract mobility data from the *m/z* regions assigned to empty and full capsids, with the 2D DT vs. *m/z* heat map allowing visualisation of the different IM profiles. The *m/z*-extracted DT data is shown on the left-hand side of the heatmap. While the empty and full capsids, as well as two partially-filled capsid species can be separated *via m/z* they exhibit similar arrival times. Prior CDMS results showed a similar average charge of full and empty particles, which is rationalised by their similar surface area.[67] Therefore, it is also expected that both particles would exhibit similar CCS. We used literature reported values for both charge (average of 155 for all capsid species) and mass (3.6 MDa for the empty capsid and 5.1 MDa for the full capsid)[67] for our estimations of CCS. From these values, the CCS was estimated to be 55,600 $Å^2$ and 58,900 $Å^2$ for empty and full capsids, respectively. The CCS values converted to radii are approximately 133 Å for empty and 137 Å for full capsids, which is in good agreement with findings from cryo-electron microscopy (EM)[68] and atomic force microscopy (AFM).[69]

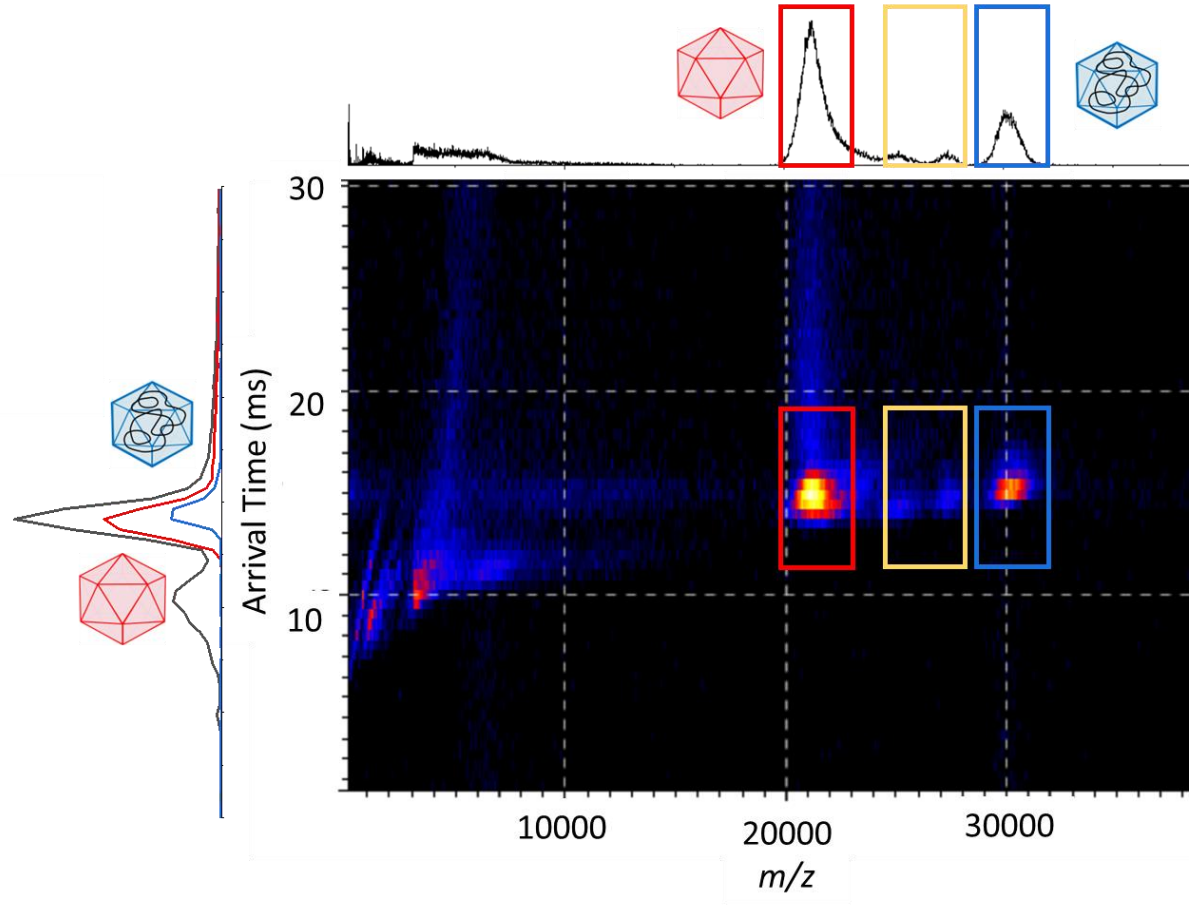

Figure 1: DTIM-MS data on empty and full AAV capsids. The mass spectrum on the top of the figure shows the empty, partially-filled and full capsids, highlighted by red, yellow and blue boxes, respectively. This data was acquired with at electric field of 6.9 V/cm and 2.2 mbar of nitrogen.

A more detailed analysis of the DTIMS data reveals subtle differences between the ATD profiles of full and empty particles (Figure 2). The width of the ATD of the empty species is larger than the width of the full species and exhibits tailing towards longer arrival times. These features suggest a larger number of conformational states attainable by the empty capsid and/or conformational rearrangements occurring on the IM separation timescale. This is consistent with dynamic light scattering (DLS) studies that show the greater polydispersity of the empty capsid versus the full.[70] While this warrants further study, we speculate that these rearrangements may be akin to an expanding and contracting motion (Figure S1). The narrower ATD of the full capsid alludes to a more constrained structure; the particles are more rigid and swollen by the incorporated genetic cargo.[71] Interestingly, the ATD of the partial 1

species exhibits width similar to that of an empty particle, while the ATD of partial 2 is more like the full particle.

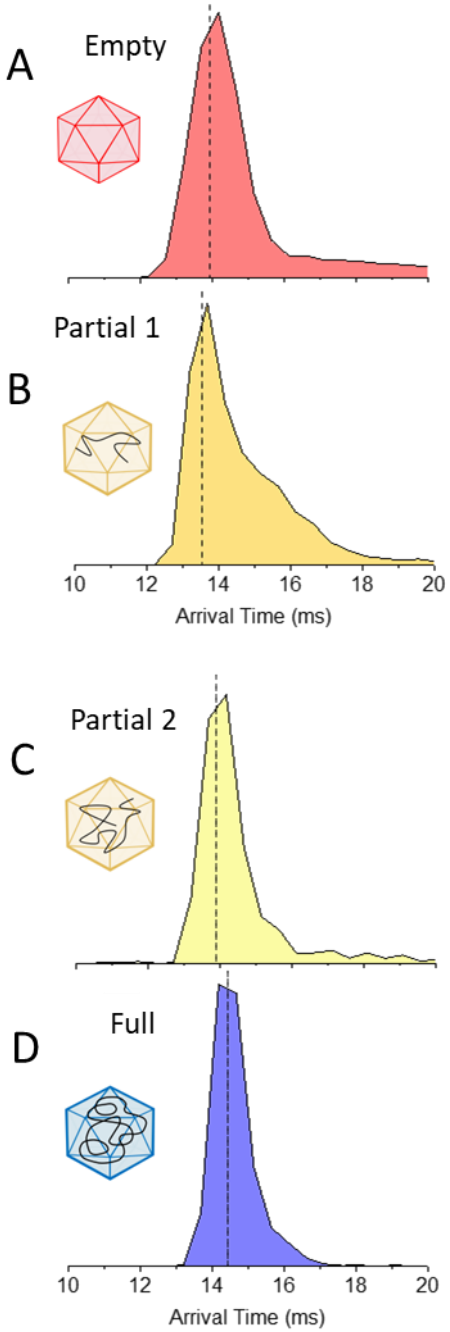

Figure 2: Detailed comparison of the ATDs of the four capsid species. The arrival time distributions (ATDs) of (A) empty, (B) partial 1, (C) partial 2 and (D) full capsids at E=6.9 V/cm, showing the conformational similarities between empty and partial 1, as well as between partial 2 and full.

TWIMS Analysis of AAV Capsids

Representative data obtained on full and empty AAV capsids using the TW separator are presented in Figure 3. The spectra in the *m/z* domain appear similar to those obtained using DTIMS, with two main peaks corresponding to full and empty capsids. Partially-filled species are not well resolved here, which may be due to the different nanoESI emitters or subtle sample preparation differences. Due to the time to switch from DT to TWIMS mode the dataset were recorded a few weeks apart, using different AAV aliquots.

Under K-dominated TW separation conditions (Figure 3A), full and empty capsids are not resolved in the arrival time dimension, resembling data obtained using DTIMS. The peak apex of the full capsid ATD is displaced from that of the empty capsid, with the empty arriving earlier. The heat map for the empty capsid presents a prolate signal, narrow in the *m/z* dimension and elongated in the arrival time dimension, indicating a wide range of conformers. The peak corresponding to full capsid presents a narrower arrival time span than the empty capsid, agreeing with our observations in DTIMS. Arrival times here increase with *m/z*. A low intensity region (yellow box) attributed to partially filled species, has a narrow spread of arrival times over a wide *m/z* range, merging with the main peak corresponding to the full capsid.

Under *m/z*-dominated TW separation conditions (Figure 3B), the separation between the ATDs of the two main capsid species is increased, compared to the K-dominated result. The partially-filled species present as a 'bridge' between the two main peaks. The empty capsid displays a narrower ATD (compared to that in Figure 3A), whereas the full capsid now arrives over a larger range of arrival times.

The DriftScope heatmap reveals that discrete distributions are not observed for the full and partially-filled species, instead a 2D band distribution with a curved form is visible. Interestingly, the 2D profile of the empty capsids clearly extends above the main band. This is indicative that conformational changes of this particle (causing decrease in K), may alter the relative influences of *m/z* and K on TW arrival time (predominately *via* reduction in α parameter). The same explanation may be used to explain complex shape of 2D profile of this particle in K-dominated TW data (i.e. Figure 3A).

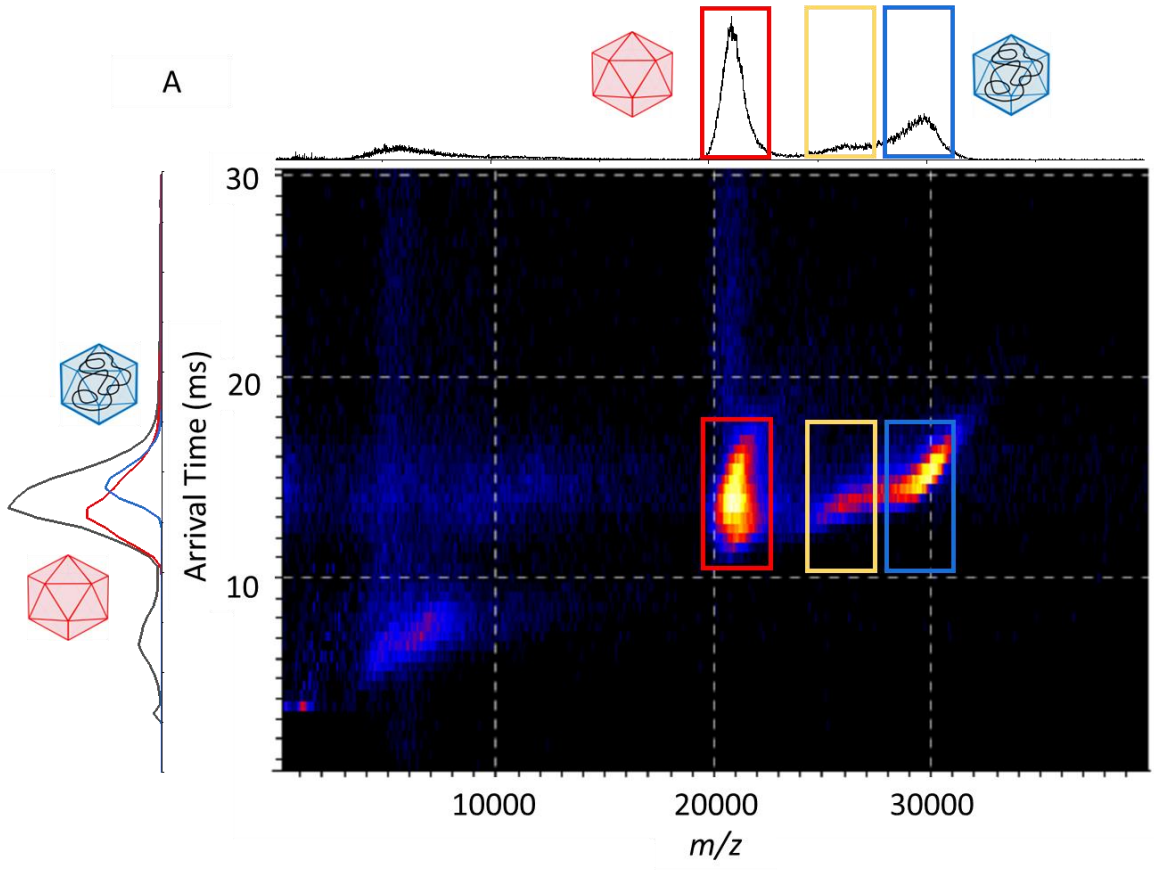

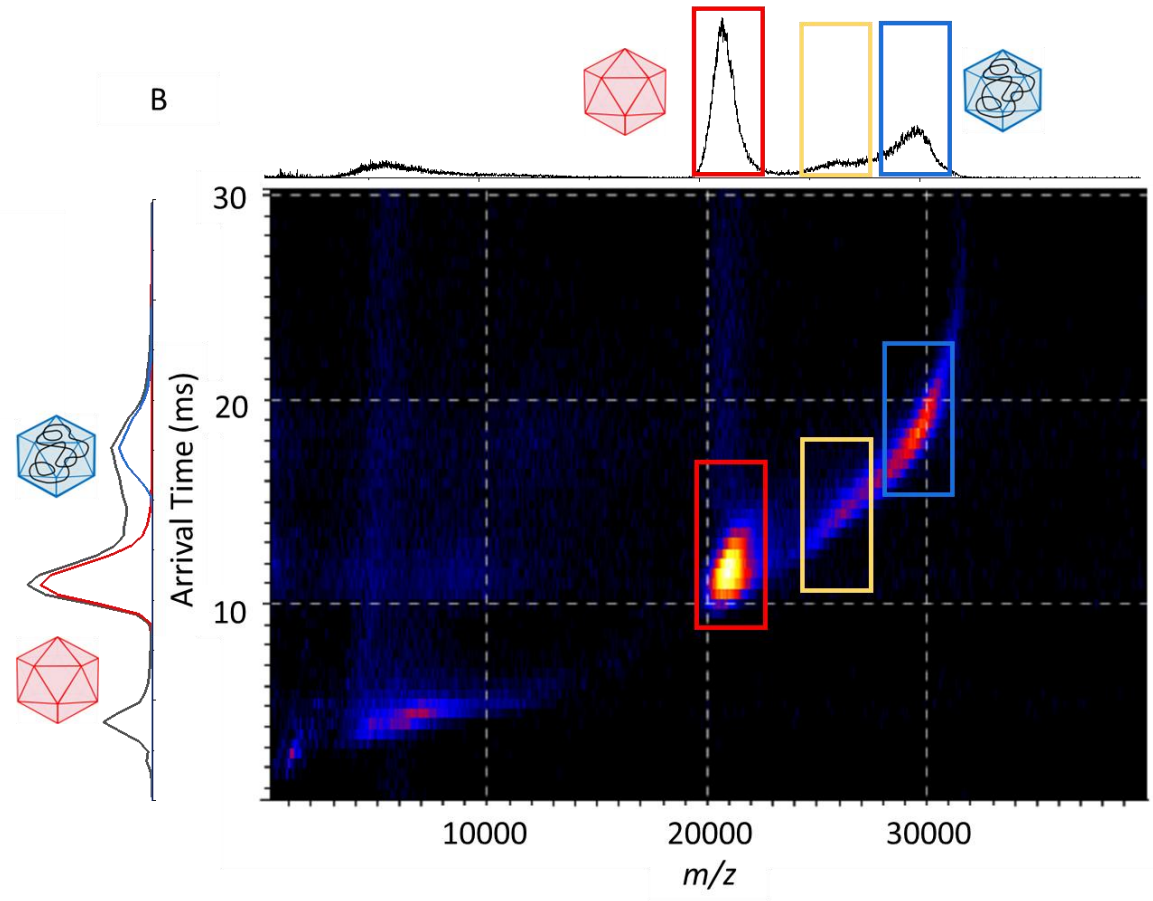

Figure 3: TW separation of AAV capsids under K- and m/z*-dominated conditions. The top traces show the mass spectrum, with empty, partially-filled and full species indicated by red, yellow and blue boxes, respectively. The black ATD trace on the left side of the heatmaps shows the total ion count, the red trace shows the* m/z *extracted ATD for the empty species and the blue trace shows the* m/z *extracted ATD for the full species. The heatmaps in the middle visualise the relationship between* m/z *and arrival time. (A) K-dominated TW separation was achieved with a TW velocity of 100 m/s and a TW height of 14 V. (B) Values for TW velocity and amplitude were increased to 320 m/s and 40 V, respectively for* m/z*-dominated TW separation. The nitrogen drift gas pressure was 2.2 mbar.*

It is evident that despite residual K-effects, *m/z* separation of full and empty particles is achievable in the 25 cm TW cell operating at 2.2 mbar and we highlight the striking similarity between *m/z*-dominated TW arrival time distribution and ToF-MS data in Figure S2. TW devices with longer separation paths and operating at lower pressures are expected to afford increased resolution of capsid forms with partial DNA. Indeed, data obtained using Cyclic IMS platform on another set of AAV samples showed resolution of partially filled capsids, comparable with ToF-MS data(Figure 4), and the 2D heatmap shows a relatively narrow 'curved' band (Figure S3). The spread in ATD is relatively small for both empty and full capsids, in line with very low influence of K on arrival time. We further investigated this trend using SIMION ion trajectory simulations. Arrival times of hypothetical particles with the same K and *z*, but varying density analogous to empty, full and partially filled capsids, within the *m/z* range 10,000 – 30,000 were simulated and are in agreement with experimental findings (Figure S4). Expectedly, the separation decreases with TW conditions resulting in lower α parameters (Table S1). It is worth noting that resolution of partial species between empty and full capsids may not be possible for all materials as packaging efficiency of AAV capsids is complex.[12] In some cases, a continuum of species may be present rather than distinct populations so orthogonal methods to confirm partial species is recommended when assessing resolution. In all, our results suggest that TW-based *m/z* separation appears adequate for quantification of the relative abundance of full and empty particles (% peak areas in insets of Figure 4), which is of high interest in gene therapy analytical laboratories.

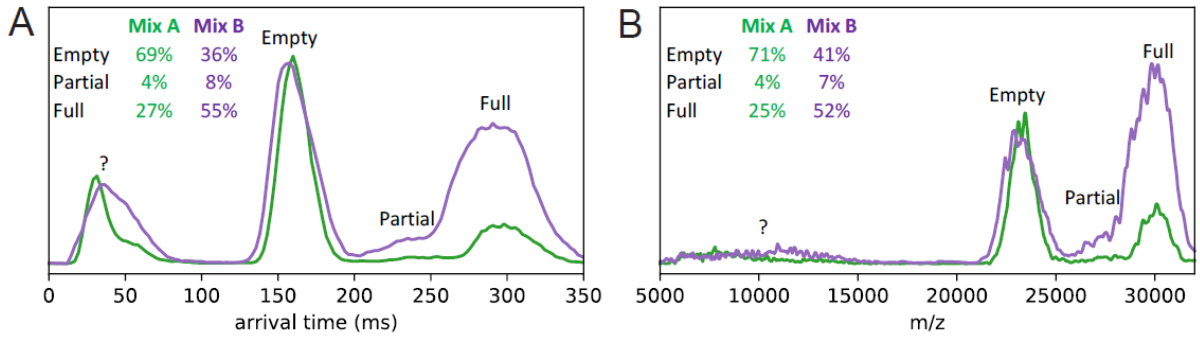

Figure 4: Comparison of (A) higher resolution m/z-dominated TW separation and (B) ToF-MS data achieved on Cyclic IMS instrument using another set of AAV samples. Two mixes of AAV capsids were assessed, mix A (green) has a higher proportion of empty species compared to full whereas mix B (purple) has the opposite, with more full species. The '?' region may pertain to a heterogeneous mix of capsid dimers and trimers etc. with DNA potentially associated that are breakdown products or intermediate species.

TWIMS theory

Considering the AAV capsid data presented here, we applied the recently described TWIMS theory from Richardson *et al.* which details the *m/z* effects in smoothly-moving TW separators.[58,60] For a given ion and a chosen set of parameters, separation characteristics of the TW device were conveniently described in terms of the dimensionless parameters α and γ:

$$\alpha = 2\pi K \frac{v}{\lambda}\frac{m}{z} \qquad \gamma = 2\pi K \frac{V_0}{v\lambda} \tag{3}$$

Where V_0 is the applied TW amplitude, v is the TW velocity and λ is the TW wavelength. For sufficiently small α (low *m/z* ions), velocity relaxation effects are negligible and average ion velocity is simplified and given by equation 4:

$$\bar{v} = v\left(1 - \sqrt{1-\gamma^2}\right) \tag{4}$$

For all α and sufficiently small γ (low TW parameters), the average ion velocity is given by equation 5:

$$\bar{v} = \frac{v}{1+\alpha^2}\left[\frac{\gamma^2}{2} + \frac{\gamma^4}{8}\frac{1+10\alpha^2+15\alpha^4}{(1+\alpha^2)^2(1+4\alpha^2)} + \frac{\gamma^6}{16}\frac{1+23\alpha^2+234\alpha^4+1171\alpha^6+2291\alpha^8+1620\alpha^{10}}{4(1+\alpha^2)^4(1+4\alpha^2)^2(1+9\alpha^2)}\right] \tag{5}$$

Therefore, for any combination of operating parameters and ion properties (i.e. α and γ), one can calculate the percentage reduction in ion velocity caused by the velocity relaxation effect (Figure 5 and Table S2). This metric can be used to quantify the relative contributions of *m/z* and K to the TW transit time. From the equations above and Figure 5, it is evident that under the appropriate TW conditions, transit time of high molecular weight ions can be dominated by *m/z*, which is of fundamental interest to measurements in TW devices.

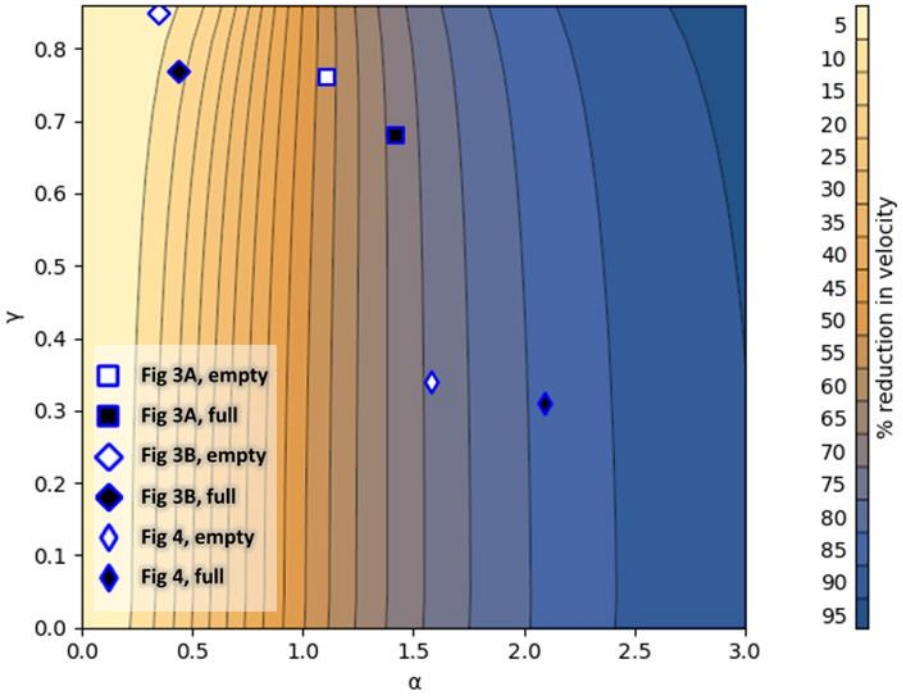

Figure 5: The percentage reduction in particle velocity caused by velocity relaxation as a function of α and γ in a smoothly-moving TW device. The symbols represent all the datasets included in this study.

Conclusions

In the present study, we explore the use of ion mobility mass spectrometry to investigate AAV capsids which are relevant in gene therapy applications. The measurement of the empty:full capsid ratio can be achieved using MS and also using TWIMS, under the appropriate conditions. We show that TW-based separation can be tailored to operate in a K-dominated regime, as well as in a *m/z*-dominated regime, the latter phenomenon being particularly interesting for separations of high molecular weight species. These findings are corroborated using the available TW theory as well as SIMION simulations. As anticipated for DTIMS (where

a ‘pure’ K-based ion transport is expected) empty and full capsid forms are not separated from each other. However, assessment of ATD distributions reveals increased structural elasticity of the empty capsid compared to the full. Not being hampered by carrying genetic material allows the empty capsid to exhibit greater conformational variation within the IMS cell, as seen with DLS studies,[70] whereas the full capsid is larger and more rigid in shape as it is packed full of DNA. This has been observed in AFM studies where a full, DNA-packed capsid showed a sphere-like structure, while an empty capsid showed a 3D ellipsoidal-like structure, with suggestions that the internal DNA is providing support to the structure of the full capsid.[69,71] We also note the evidence of these capsid differences in TW data, although it is confounded by K and *m/z* influences on TW transit time. It remains to be seen whether AAV particles of other serotypes or those with varying viral protein ratios would exhibit a similar degree of structural variability. Additionally, DTIMS allows characterisation of the partially filled capsid species as either empty-like or full-like, based on the ATDs. The ability of IMS to probe the conformations of these caged structures offers promise for the study of other such analytes using this method. In all, the IM-MS methods presented in this study offer a quick, simple and reliable assessment of AAV quality attributes and should be suitable for adoption in the biopharmaceutical industry.

Acknowledgements

We acknowledge the support of EPSRC through the strategic equipment award EP/T019328/1 and for the Prosperity Partnership award EP/S005226/1, the BBSRC for the award BB/X002403/1 and Waters Corporation for their continued support of mass spectrometry research within the Michael Barber Centre for Collaborative Mass Spectrometry. EL. acknowledges the BBSRC DTP and Pharamron Ltd. for funding a strategic CASE studentship. The authors also thank the staff in the MS and Separation Science facility, in the faculty of Science and Engineering for their continued assistance.

Conflict of Interest Statement

KR, DL, KG and JU are employees of Waters Corporation and may own stock or share options. PG and MW are employees of Pharmaron Biologics Ltd. and may own stock or share options.

References

(1) Vandendriessche, T.; Thorrez, L.; Acosta-Sanchez, A.; Petrus, I.; Wang, L.; Ma, L.; De Waele, L.; Iwasaki, Y.; Gillijns, V.; Wilson, J. M.; Collen, D.; Chuah, M. K. L. Efficacy and Safety of Adeno-Associated Viral Vectors Based on Serotype 8 and 9 vs. Lentiviral Vectors for Hemophilia B Gene Therapy. *Journal of Thrombosis and Haemostasis* **2007**, *5* (1), 16–24. https://doi.org/10.1111/j.1538-7836.2006.02220.x.

(2) Mueller, C.; Flotte, T. R. Clinical Gene Therapy Using Recombinant Adeno-Associated Virus Vectors. *Gene Ther* **2008**, *15* (11), 858–863. https://doi.org/10.1038/gt.2008.68.

(3) Naso, M. F.; Tomkowicz, B.; Perry, W. L.; Strohl, W. R. Adeno-Associated Virus (AAV) as a Vector for Gene Therapy. *BioDrugs* **2017**, *31* (4), 317–334. https://doi.org/10.1007/s40259-017-0234-5.

(4) Becerra, S. P.; Koczot, F.; Fabisch, P.; Rose, J. A. Synthesis of Adeno-Associated Virus Structural Proteins Requires Both Alternative mRNA Splicing and Alternative Initiations from a Single Transcript. *J Virol* **1988**, *62* (8), 2745–2754.

(5) Trempe, J. P.; Carter, B. J. Alternate mRNA Splicing Is Required for Synthesis of Adeno-Associated Virus VP1 Capsid Protein. *J Virol* **1988**, *62* (9), 3356–3363.

(6) Mietzsch, M.; Pénzes, J. J.; Agbandje-McKenna, M. Twenty-Five Years of Structural Parvovirology. *Viruses* **2019**, *11* (4), 362. https://doi.org/10.3390/v11040362.

(7) Pillay, S.; Zou, W.; Cheng, F.; Puschnik, A. S.; Meyer, N. L.; Ganaie, S. S.; Deng, X.; Wosen, J. E.; Davulcu, O.; Yan, Z.; Engelhardt, J. F.; Brown, K. E.; Chapman, M. S.; Qiu, J.; Carette, J. E. Adeno-Associated Virus (AAV) Serotypes Have Distinctive Interactions with Domains of the Cellular AAV Receptor. *Journal of Virology* **2017**, *91* (18), e00391-17. https://doi.org/10.1128/JVI.00391-17.

(8) Schmidt, M.; Govindasamy, L.; Afione, S.; Kaludov, N.; Agbandje-McKenna, M.; Chiorini, J. A. Molecular Characterization of the Heparin-Dependent Transduction Domain on the Capsid of a Novel Adeno-Associated Virus Isolate, AAV(VR-942). *J Virol* **2008**, *82* (17), 8911–8916. https://doi.org/10.1128/JVI.00672-08.

(9) Zincarelli, C.; Soltys, S.; Rengo, G.; Rabinowitz, J. E. Analysis of AAV Serotypes 1–9 Mediated Gene Expression and Tropism in Mice After Systemic Injection. *Molecular Therapy* **2008**, *16* (6), 1073–1080. https://doi.org/10.1038/mt.2008.76.

(10) European Medicines Agency, C. for B. E. and R. Guideline on the Quality, Non-Clinical and Clinical Aspects of Gene Therapy Medicinal Products, 2018. https://www.ema.europa.eu/en/documents/scientific-guideline/guideline-quality-non-clinical-clinical-aspects-gene-therapy-medicinal-products_en.pdf.

(11) Food and Drug Administration, U. S. D. of H. and H. S. Chemistry, Manufacturing, and Control (CMC) Information for Human Gene Therapy Investigational New Drug Applications (INDs), 2020. https://www.fda.gov/media/113760/download (accessed 2023-02-21).

(12) Ebberink, E. H. T. M.; Ruisinger, A.; Nuebel, M.; Thomann, M.; Heck, A. J. R. Assessing Production Variability in Empty and Filled Adeno-Associated Viruses by Single Molecule Mass Analyses. *Molecular Therapy Methods & Clinical Development* **2022**, *27*, 491–501. https://doi.org/10.1016/j.omtm.2022.11.003.

(13) Wu, Z.; Yang, H.; Colosi, P. Effect of Genome Size on AAV Vector Packaging. *Mol Ther* **2010**, *18* (1), 80–86. https://doi.org/10.1038/mt.2009.255.

(14) Strasser, L.; Morgan, T. E.; Guapo, F.; Füssl, F.; Forsey, D.; Anderson, I.; Bones, J. A Native Mass Spectrometry-Based Assay for Rapid Assessment of the Empty:Full Capsid Ratio in Adeno-Associated Virus Gene Therapy Products. *Analytical Chemistry* **2021**, *93* (38), 12817–12821. https://doi.org/10.1021/acs.analchem.1c02828.

(15) McColl-Carboni, A.; Dollive, S.; Laughlin, S.; Lushi, R.; MacArthur, M.; Zhou, S.; Gagnon, J.; Smith, C. A.; Burnham, B.; Horton, R.; Lata, D.; Uga, B.; Natu, K.; Michel, E.; Slater, C.;

DaSilva, E.; Bruccoleri, R.; Kelly, T.; McGivney, J. B. Analytical Characterization of Full, Intermediate, and Empty AAV Capsids. *Gene Ther* **2024**, 1–10. https://doi.org/10.1038/s41434-024-00444-2.

(16) Henrickson, A.; Ding, X.; Seal, A. G.; Qu, Z.; Tomlinson, L.; Forsey, J.; Gradinaru, V.; Oka, K.; Demeler, B. Characterization and Quantification of Adeno-Associated Virus Capsid-Loading States by Multi-Wavelength Analytical Ultracentrifugation with UltraScan. *Nanomedicine (Lond)* **2023**, *18* (22), 1519–1534. https://doi.org/10.2217/nnm-2023-0156.

(17) McIntosh, N. L.; Berguig, G. Y.; Karim, O. A.; Cortesio, C. L.; De Angelis, R.; Khan, A. A.; Gold, D.; Maga, J. A.; Bhat, V. S. Comprehensive Characterization and Quantification of Adeno Associated Vectors by Size Exclusion Chromatography and Multi Angle Light Scattering. *Sci Rep* **2021**, *11* (1), 3012. https://doi.org/10.1038/s41598-021-82599-1.

(18) Burnham, B.; Nass, S.; Kong, E.; Mattingly, M.; Woodcock, D.; Song, A.; Wadsworth, S.; Cheng, S. H.; Scaria, A.; O'Riordan, C. R. Analytical Ultracentrifugation as an Approach to Characterize Recombinant Adeno-Associated Viral Vectors. *Human Gene Therapy Methods* **2015**, *26* (6), 228–242. https://doi.org/10.1089/hgtb.2015.048.

(19) Werle, A. K.; Powers, T. W.; Zobel, J. F.; Wappelhorst, C. N.; Jarrold, M. F.; Lyktey, N. A.; Sloan, C. D. K.; Wolf, A. J.; Adams-Hall, S.; Baldus, P.; Runnels, H. A. Comparison of Analytical Techniques to Quantitate the Capsid Content of Adeno-Associated Viral Vectors. *Molecular Therapy - Methods & Clinical Development* **2021**, *23*, 254–262. https://doi.org/10.1016/j.omtm.2021.08.009.

(20) Loo, J. A. Electrospray Ionization Mass Spectrometry: A Technology for Studying Noncovalent Macromolecular Complexes. *International Journal of Mass Spectrometry* **2000**, *200* (1), 175–186. https://doi.org/10.1016/S1387-3806(00)00298-0.

(21) Sobott, F.; Robinson, C. V. Protein Complexes Gain Momentum. *Current Opinion in Structural Biology* **2002**, *12* (6), 729–734. https://doi.org/10.1016/S0959-440X(02)00400-1.

(22) Ashcroft, A. E. Mass Spectrometry-Based Studies of Virus Assembly. *Current Opinion in Virology* **2019**, *36*, 17–24. https://doi.org/10.1016/j.coviro.2019.02.006.

(23) Knapman, T. W.; Morton, V. L.; Stonehouse, N. J.; Stockley, P. G.; Ashcroft, A. E. Determining the Topology of Virus Assembly Intermediates Using Ion Mobility Spectrometry–Mass Spectrometry. *Rapid Communications in Mass Spectrometry* **2010**, *24* (20), 3033–3042. https://doi.org/10.1002/rcm.4732.

(24) Lutomski, C. A.; Lyktey, N. A.; Pierson, E. E.; Zhao, Z.; Zlotnick, A.; Jarrold, M. F. Multiple Pathways in Capsid Assembly. *J. Am. Chem. Soc.* **2018**, *140* (17), 5784–5790. https://doi.org/10.1021/jacs.8b01804.

(25) Pogan, R.; Dülfer, J.; Uetrecht, C. Norovirus Assembly and Stability. *Current Opinion in Virology* **2018**, *31*, 59–65. https://doi.org/10.1016/j.coviro.2018.05.003.

(26) Tamara, S.; den Boer, M. A.; Heck, A. J. R. High-Resolution Native Mass Spectrometry. *Chem. Rev.* **2022**, *122* (8), 7269–7326. https://doi.org/10.1021/acs.chemrev.1c00212.

(27) Tito, M. A.; Tars, K.; Valegard, K.; Hajdu, J.; Robinson, C. V. Electrospray Time-of-Flight Mass Spectrometry of the Intact MS2 Virus Capsid. *J. Am. Chem. Soc.* **2000**, *122* (14), 3550–3551. https://doi.org/10.1021/ja993740k.

(28) Snijder, J.; Rose, R. J.; Veesler, D.; Johnson, J. E.; Heck, A. J. R. Studying 18 Mega Dalton Virus Assemblies with Native Mass Spectrometry. *Angew Chem Int Ed Engl* **2013**, *52* (14), 4020–4023. https://doi.org/10.1002/anie.201210197.

(29) Bereszczak, J. Z.; Rose, R. J.; van Duijn, E.; Watts, N. R.; Wingfield, P. T.; Steven, A. C.; Heck, A. J. R. Epitope-Distal Effects Accompany the Binding of Two Distinct Antibodies to Hepatitis B Virus Capsids. *J. Am. Chem. Soc.* **2013**, *135* (17), 6504–6512. https://doi.org/10.1021/ja402023x.

(30) Liu, A. P.; Patel, S. K.; Xing, T.; Yan, Y.; Wang, S.; Li, N. Characterization of Adeno-Associated Virus Capsid Proteins Using Hydrophilic Interaction Chromatography Coupled

with Mass Spectrometry. *Journal of Pharmaceutical and Biomedical Analysis* **2020**, *189*, 113481. https://doi.org/10.1016/j.jpba.2020.113481.
(31) Contino, N. C.; Jarrold, M. F. Charge Detection Mass Spectrometry for Single Ions with a Limit of Detection of 30 Charges. *International Journal of Mass Spectrometry* **2013**, *345–347*, 153–159. https://doi.org/10.1016/j.ijms.2012.07.010.
(32) Kafader, J. O.; Melani, R. D.; Durbin, K. R.; Ikwuagwu, B.; Early, B. P.; Fellers, R. T.; Beu, S. C.; Zabrouskov, V.; Makarov, A. A.; Maze, J. T.; Shinholt, D. L.; Yip, P. F.; Tullman-Ercek, D.; Senko, M. W.; Compton, P. D.; Kelleher, N. L. Multiplexed Mass Spectrometry of Individual Ions Improves Measurement of Proteoforms and Their Complexes. *Nat Methods* **2020**, *17* (4), 391–394. https://doi.org/10.1038/s41592-020-0764-5.
(33) Wörner, T. P.; Snijder, J.; Bennett, A.; Agbandje-McKenna, M.; Makarov, A. A.; Heck, A. J. R. Resolving Heterogeneous Macromolecular Assemblies by Orbitrap-Based Single-Particle Charge Detection Mass Spectrometry. *Nat Methods* **2020**, *17* (4), 395–398. https://doi.org/10.1038/s41592-020-0770-7.
(34) Wörner, T. P.; Bennett, A.; Habka, S.; Snijder, J.; Friese, O.; Powers, T.; Agbandje-McKenna, M.; Heck, A. J. R. Adeno-Associated Virus Capsid Assembly Is Divergent and Stochastic. *Nat Commun* **2021**, *12*, 1642. https://doi.org/10.1038/s41467-021-21935-5.
(35) Snijder, J.; van de Waterbeemd, M.; Damoc, E.; Denisov, E.; Grinfeld, D.; Bennett, A.; Agbandje-McKenna, M.; Makarov, A.; Heck, A. J. R. Defining the Stoichiometry and Cargo Load of Viral and Bacterial Nanoparticles by Orbitrap Mass Spectrometry. *J. Am. Chem. Soc.* **2014**, *136* (20), 7295–7299. https://doi.org/10.1021/ja502616y.
(36) Ujma, J.; Giles, K.; Anderson, M.; Richardson, K. Enhanced Declustering and Charge-Stripping Enables Mass Determination of AAVs in TOF MS. *ASMS* **2022**.
(37) Huray, K. I. P. L.; Wörner, T. P.; Moreira, T.; Reinhardt-Szyba, M.; Devine, P. W. A.; Bond, N. J.; Fort, K. L.; Makarov, A. A.; Sobott, F. To 200,000 *m/z* and beyond: Native Electron Capture Charge Reduction Mass Spectrometry Deconvolves Heterogeneous Signals in Large Biopharmaceutical Analytes. bioRxiv February 19, 2024, p 2024.02.19.581059. https://doi.org/10.1101/2024.02.19.581059.
(38) Kostelic, M. M.; Ryan, J. P.; Brown, L. S.; Jackson, T. W.; Hsieh, C.-C.; Zak, C. K.; Sanders, H. M.; Liu, Y.; Chen, V. S.; Byrne, M.; Aspinwall, C. A.; Baker, E. S.; Marty, M. T. Stability and Dissociation of Adeno-Associated Viral Capsids by Variable Temperature-Charge Detection-Mass Spectrometry. *Anal. Chem.* **2022**, *94* (34), 11723–11727. https://doi.org/10.1021/acs.analchem.2c02378.
(39) Barnes, L. F.; Draper, B. E.; Kurian, J.; Chen, Y.-T.; Shapkina, T.; Powers, T. W.; Jarrold, M. F. Analysis of AAV-Extracted DNA by Charge Detection Mass Spectrometry Reveals Genome Truncations. *Anal. Chem.* **2023**, *95* (9), 4310–4316. https://doi.org/10.1021/acs.analchem.2c04234.
(40) Christofi, E.; Barran, P. Ion Mobility Mass Spectrometry (IM-MS) for Structural Biology: Insights Gained by Measuring Mass, Charge, and Collision Cross Section. *Chem Rev* **2023**. https://doi.org/10.1021/acs.chemrev.2c00600.
(41) Gabelica, V.; Marklund, E. Fundamentals of Ion Mobility Spectrometry. *Current Opinion in Chemical Biology* **2018**, *42*, 51–59. https://doi.org/10.1016/j.cbpa.2017.10.022.
(42) McDaniel, E. W.; Mason, E. A. *Mobility and Diffusion of Ions in Gases*; John Wiley and Sons, Inc: United States, 1973.
(43) Mason, E. A.; Schamp, H. W. Mobility of Gaseous Lons in Weak Electric Fields. *Annals of Physics* **1958**, *4* (3), 233–270. https://doi.org/10.1016/0003-4916(58)90049-6.
(44) France, A. P.; Migas, L. G.; Sinclair, E.; Bellina, B.; Barran, P. E. Using Collision Cross Section Distributions to Assess the Distribution of Collision Cross Section Values. *Anal. Chem.* **2020**, *92* (6), 4340–4348. https://doi.org/10.1021/acs.analchem.9b05130.
(45) Stow, S. M.; Causon, T. J.; Zheng, X.; Kurulugama, R. T.; Mairinger, T.; May, J. C.; Rennie, E. E.; Baker, E. S.; Smith, R. D.; McLean, J. A.; Hann, S.; Fjeldsted, J. C. An Interlaboratory

Evaluation of Drift Tube Ion Mobility - Mass Spectrometry Collision Cross Section Measurements. *Anal Chem* **2017**, *89* (17), 9048–9055. https://doi.org/10.1021/acs.analchem.7b01729.
(46) McCabe, J. W.; Hebert, M. J.; Shirzadeh, M.; Mallis, C. S.; Denton, J. K.; Walker, T. E.; Russell, D. H. THE IMS PARADOX: A PERSPECTIVE ON STRUCTURAL ION MOBILITY-MASS SPECTROMETRY. *Mass Spectrom Rev* **2021**, *40* (3), 280–305. https://doi.org/10.1002/mas.21642.
(47) Gerlich, D. Inhomogeneous RF Fields: A Versatile Tool for the Study of Processes with Slow Ions. In *Advances in Chemical Physics*; John Wiley & Sons, Ltd, 1992; pp 1–176. https://doi.org/10.1002/9780470141397.ch1.
(48) Ibrahim, Y.; Tang, K.; Tolmachev, A. V.; Shvartsburg, A. A.; Smith, R. D. Improving Mass Spectrometer Sensitivity Using a High-Pressure Electrodynamic Ion Funnel Interface. *Journal of the American Society for Mass Spectrometry* **2006**, *17* (9), 1299–1305. https://doi.org/10.1016/j.jasms.2006.06.005.
(49) Kemper, P. R.; Dupuis, N. F.; Bowers, M. T. A New, Higher Resolution, Ion Mobility Mass Spectrometer. *International Journal of Mass Spectrometry* **2009**, *287* (1), 46–57. https://doi.org/10.1016/j.ijms.2009.01.012.
(50) Allen, S. J.; Giles, K.; Gilbert, T.; Bush, M. F. Ion Mobility Mass Spectrometry of Peptide, Protein, and Protein Complex Ions Using a Radio-Frequency Confining Drift Cell. *Analyst* **2016**, *141* (3), 884–891. https://doi.org/10.1039/C5AN02107C.
(51) Upton, R.; Migas, L. G.; Pacholarz, K. J.; Beniston, R. G.; Estdale, S.; Firth, D.; Barran, P. E. Hybrid Mass Spectrometry Methods Reveal Lot-to-Lot Differences and Delineate the Effects of Glycosylation on the Tertiary Structure of Herceptin®. *Chem. Sci.* **2019**, *10* (9), 2811–2820. https://doi.org/10.1039/C8SC05029E.
(52) Ujma, J.; Giles, K.; Morris, M.; Barran, P. E. New High Resolution Ion Mobility Mass Spectrometer Capable of Measurements of Collision Cross Sections from 150 to 520 K. *Anal. Chem.* **2016**, *88* (19), 9469–9478. https://doi.org/10.1021/acs.analchem.6b01812.
(53) Ujma, J.; Jhingree, J.; Norgate, E.; Upton, R.; Wang, X.; Benoit, F.; Bellina, B.; Barran, P. Protein Unfolding in Freeze Frames: Intermediate States Are Revealed by Variable-Temperature Ion Mobility–Mass Spectrometry. *Anal Chem* **2022**, *94* (35), 12248–12255. https://doi.org/10.1021/acs.analchem.2c03066.
(54) Pacholarz, K. J.; Barran, P. E. Distinguishing Loss of Structure from Subunit Dissociation for Protein Complexes with Variable Temperature Ion Mobility Mass Spectrometry. *Anal. Chem.* **2015**, *87* (12), 6271–6279. https://doi.org/10.1021/acs.analchem.5b01063.
(55) Pringle, S. D.; Giles, K.; Wildgoose, J. L.; Williams, J. P.; Slade, S. E.; Thalassinos, K.; Bateman, R. H.; Bowers, M. T.; Scrivens, J. H. An Investigation of the Mobility Separation of Some Peptide and Protein Ions Using a New Hybrid Quadrupole/Travelling Wave IMS/Oa-ToF Instrument. *International Journal of Mass Spectrometry* **2007**, *261* (1), 1–12. https://doi.org/10.1016/j.ijms.2006.07.021.
(56) Ruotolo, B. T.; Giles, K.; Campuzano, I.; Sandercock, A. M.; Bateman, R. H.; Robinson, C. V. Evidence for Macromolecular Protein Rings in the Absence of Bulk Water. *Science* **2005**, *310* (5754), 1658–1661. https://doi.org/10.1126/science.1120177.
(57) Johnsen, R.; Biondi, M. A. Reaction Rates of Uranium Ions and Atoms with O2 and N2. *The Journal of Chemical Physics* **1972**, *57* (5), 1975–1979. https://doi.org/10.1063/1.1678517.
(58) Richardson, K.; Langridge, D.; Giles, K. Fundamentals of Travelling Wave Ion Mobility Revisited: I. Smoothly Moving Waves. *International Journal of Mass Spectrometry* **2018**, *428*, 71–80. https://doi.org/10.1016/j.ijms.2018.03.007.
(59) Gabelica, V.; Shvartsburg, A. A.; Afonso, C.; Barran, P.; Benesch, J. L. P.; Bleiholder, C.; Bowers, M. T.; Bilbao, A.; Bush, M. F.; Campbell, J. L.; Campuzano, I. D. G.; Causon, T.; Clowers, B. H.; Creaser, C. S.; De Pauw, E.; Far, J.; Fernandez-Lima, F.; Fjeldsted, J. C.; Giles, K.; Groessl, M.; Hogan Jr, C. J.; Hann, S.; Kim, H. I.; Kurulugama, R. T.; May, J. C.;

McLean, J. A.; Pagel, K.; Richardson, K.; Ridgeway, M. E.; Rosu, F.; Sobott, F.; Thalassinos, K.; Valentine, S. J.; Wyttenbach, T. Recommendations for Reporting Ion Mobility Mass Spectrometry Measurements. *Mass Spectrometry Reviews* **2019**, *38* (3), 291–320. https://doi.org/10.1002/mas.21585.

(60) Richardson, K.; Langridge, D.; Dixit, S. M.; Ruotolo, B. T. An Improved Calibration Approach for Traveling Wave Ion Mobility Spectrometry: Robust, High-Precision Collision Cross Sections. *Anal. Chem.* **2021**, *93* (7), 3542–3550. https://doi.org/10.1021/acs.analchem.0c04948.

(61) Giles, K.; Pringle, S. D.; Wildgoose, J. L.; Bateman, R. H. A Travelling Wave-Based Ion Mobility Separator. In *54th ASMS Conference on Mass Spectrometry and Allied Topics*; Seattle, WA, 2006.

(62) Giles, K.; Pringle, S. D.; Worthington, K. R.; Little, D.; Wildgoose, J. L.; Bateman, R. H. Applications of a Travelling Wave-Based Radio-Frequency-Only Stacked Ring Ion Guide. *Rapid Communications in Mass Spectrometry* **2004**, *18* (20), 2401–2414. https://doi.org/10.1002/rcm.1641.

(63) Devine, P. W. A.; Fisher, H. C.; Calabrese, A. N.; Whelan, F.; Higazi, D. R.; Potts, J. R.; Lowe, D. C.; Radford, S. E.; Ashcroft, A. E. Investigating the Structural Compaction of Biomolecules Upon Transition to the Gas-Phase Using ESI-TWIMS-MS. *J Am Soc Mass Spectrom* **2017**, *28* (9), 1855–1862. https://doi.org/10.1007/s13361-017-1689-9.

(64) Pacholarz, K. J.; Porrini, M.; Garlish, R. A.; Burnley, R. J.; Taylor, R. J.; Henry, A. J.; Barran, P. E. Dynamics of Intact Immunoglobulin G Explored by Drift-Tube Ion-Mobility Mass Spectrometry and Molecular Modeling. *Angewandte Chemie International Edition* **2014**, *53* (30), 7765–7769. https://doi.org/10.1002/anie.201402863.

(65) Uetrecht, C.; Barbu, I. M.; Shoemaker, G. K.; van Duijn, E.; Heck, A. J. R. Interrogating Viral Capsid Assembly with Ion Mobility–Mass Spectrometry. *Nature Chem* **2011**, *3* (2), 126–132. https://doi.org/10.1038/nchem.947.

(66) Appelhans, A. D.; Dahl, D. A. SIMION Ion Optics Simulations at Atmospheric Pressure. *International Journal of Mass Spectrometry* **2005**, *244* (1), 1–14. https://doi.org/10.1016/j.ijms.2005.03.010.

(67) Pierson, E. E.; Keifer, David. Z.; Asokan, A.; Jarrold, M. F. Resolving Adeno-Associated Viral Particle Diversity With Charge Detection Mass Spectrometry. *Anal Chem* **2016**, *88* (13), 6718–6725. https://doi.org/10.1021/acs.analchem.6b00883.

(68) Silveria, M. A.; Large, E. E.; Zane, G. M.; White, T. A.; Chapman, M. S. The Structure of an AAV5-AAVR Complex at 2.5 Å Resolution: Implications for Cellular Entry and Immune Neutralization of AAV Gene Therapy Vectors. *Viruses* **2020**, *12* (11), 1326. https://doi.org/10.3390/v12111326.

(69) Nam, Y. R.; Ju, H. H.; Lee, J.; Lee, D.; Kim, Y.; Lee, S. J.; Kim, H. K.; Jang, J.-H.; Lee, H. Distinguishing between DNA-Loaded Full and Empty Capsids of Adeno-Associated Virus with Atomic Force Microscopy Imaging. *Langmuir* **2023**, *39* (19), 6740–6747. https://doi.org/10.1021/acs.langmuir.3c00241.

(70) Cole, L.; Fernandes, D.; Hussain, M. T.; Kaszuba, M.; Stenson, J.; Markova, N. Characterization of Recombinant Adeno-Associated Viruses (rAAVs) for Gene Therapy Using Orthogonal Techniques. *Pharmaceutics* **2021**, *13* (4), 586. https://doi.org/10.3390/pharmaceutics13040586.

(71) Zeng, C.; Moller-Tank, S.; Asokan, A.; Dragnea, B. Probing the Link among Genomic Cargo, Contact Mechanics, and Nanoindentation in Recombinant Adeno-Associated Virus 2. *J. Phys. Chem. B* **2017**, *121* (8), 1843–1853. https://doi.org/10.1021/acs.jpcb.6b10131.